NANO LETTERS

2006
Vol. 6, No. 4
735−739

Ferroelectric Phase Transition in Individual Single-Crystalline $BaTiO_3$ Nanowires

Jonathan E. Spanier,[†,§,||] Alexie M. Kolpak,[†,⊥] Jeffrey J. Urban,[§] Ilya Grinberg,[⊥] Lian Ouyang,[§] Wan Soo Yun,[‡,§] Andrew M. Rappe,*[,⊥] and Hongkun Park*[,§]

Department of Chemistry and Chemical Biology, Harvard University, Cambridge Massachusetts 02138, Department of Materials Science and Engineering, Drexel University, Philadelphia, Pennsylvania 19104, and The Makineni Theoretical Laboratories, Department of Chemistry, University of Pennsylvania, Philadelphia, Pennsylvania 19104-6323

Received December 24, 2005

ABSTRACT

We report scanned probe characterizations of the ferroelectric phase transition in individual barium titanate ($BaTiO_3$) nanowires. Variable-temperature electrostatic force microscopy is used to manipulate, image, and evaluate the diameter-dependent stability of ferroelectric polarizations. These measurements show that the ferroelectric phase transition temperature (T_C) is depressed as the nanowire diameter (d_{nw}) decreases, following a $1/d_{nw}$ scaling. The diameter at which T_C falls below room temperature is determined to be ~3 nm, and extrapolation of the data indicates that nanowires with d_{nw} as small as 0.8 nm can support ferroelectricity at lower temperatures. We also present density functional theory (DFT) calculations of bare and molecule-covered $BaTiO_3$ surfaces. These calculations indicate that ferroelectricity in nanowires is stabilized by molecular adsorbates such as OH and carboxylates. These adsorbates are found to passivate polarization charge more effectively than metallic electrodes, explaining the observed stability of ferroelectricity in small-diameter $BaTiO_3$ nanowires.

Ferroelectric phase transitions of perovskite-based oxides represent an important class of structural phase transitions that bear significant technological implications.[1,2] Ferroelectric perovskites exhibit a spontaneous electric polarization that can be reoriented by an external electric field.[1,2] As the temperature increases and reaches a critical temperature, T_C, these oxides undergo a polar-to-centrosymmetric structural transformation. The size dependence of T_C governs the ultimate size limit of ferroelectric nonvolatile memory[3,4] and has been the subject of numerous investigations.[5−12]

One of the most important factors determining the stability of nanoscale ferroelectricity is the compensation of polarization-induced surface charges.[1,2] Incomplete screening of surface charges results in a depolarization field that opposes the bulk polarization, thereby suppressing ferroelectricity. In typical ferroelectric devices, the surface charge is screened by two metallic electrodes that sandwich the ferroelectric material.[1,2] The observations of stable ferroelectricity in thin ferroelectric films[5−7,13−15] and nanocrystalline materials[11,12] in the absence of metallic electrodes suggest, however, that other screening mechanisms may also be operative in stabilizing nanoscale ferroelectricity.

Here, we report combined experimental and theoretical investigations that characterize nanoscale ferroelectricity in single-crystalline $BaTiO_3$ nanowires and propose a new mechanism for the screening of surface charge by atomic and molecular adsorbates. Variable-temperature scanned probe microscopy is used to probe temperature-induced phase transitions in individual single-crystalline $BaTiO_3$ nanowires lying on gold (Au) substrates, thereby removing the difficulties associated with ensemble averaging.[11,12] Our density functional theory (DFT) calculations and first-principles statistical mechanical modeling[16,17] indicate that charge compensation is provided by molecular hydroxyl (OH) and/or carboxylate (R−COO) adsorbates, which are prevalent on oxide surfaces[16,18−20] and confirmed to be present in our experiments. Our theoretical calculations show that these adsorbates provide more effective charge screening than metallic and oxide electrodes,[9,10] stabilizing ferroelectricity in smaller $BaTiO_3$ structures. These findings suggest that perovskite-based ferroelectric devices can be miniaturized

* To whom correspondence should be addressed. E-mail: rappe@sas.upenn.edu; Hongkun_Park@harvard.edu.
† These authors contributed equally to this work.
‡ Present Address: Korea Research Institute of Standards and Science, Daejeon, Republic of Korea.
§ Harvard University.
|| Drexel University.
⊥ University of Pennsylvania.

10.1021/nl052538e CCC: $33.50
Published on Web 03/15/2006

further than imagined previously by exploiting the new charge compensation mechanism.

The single-crystalline $BaTiO_3$ nanowires were synthesized by solution-phase decomposition of barium titanium isopropoxide as reported previously.[21] The procedure yields well-isolated $BaTiO_3$ nanowires with diameters ranging from 3 to 100 nm and lengths up to and above 10 μm. Electron microscopy and converging beam electron diffraction measurements show that these nanowires possess a single-crystalline perovskite structure with a principal axis lying along the nanowire length.

The ferroelectric properties of individual $BaTiO_3$ nanowires were investigated by dispersing them onto a Au substrate and probing them using a variable-temperature scanned probe microscope (SPM) in an ultrahigh-vacuum environment (base pressure $\sim 10^{-10}$ Torr), as reported previously.[22] Topographic images of the nanowires were obtained by operating the SPM in a noncontact atomic force microscopy (AFM) mode. Once a nanowire was located and its diameter (d_{nw}) was measured, ferroelectric polarization was induced or "written" on the nanowire (perpendicular to the wire axis) by applying a large voltage (V_{tip}) to a conductive SPM tip. The written polarization was then probed or "read" using electrostatic force microscopy (EFM) by measuring the shift ($\Delta\nu$) in the cantilever resonance frequency while scanning the tip with a small V_{tip}.[1,5,13−15,22]

The actual polarization maps were obtained by subtracting an EFM image at $V_{tip} = +1.5$ V from another taken at $V_{tip} = -1.5$ V, as shown in Figure 1b. This procedure eliminates the capacitive contribution between the tip and the nanowire so that the resulting map exhibits only the contribution from the surface charges associated with a local electric polarization. Specifically, the contrast in an EFM image reflects the variation in the electrostatic potential across the surface of the nanowire arising from the presence of localized surface charges, a finite-range dipole layer, and/or variations in the work function. Previous studies have shown that the lateral extent of the polarized domain does not affect the behavior of the nanowires significantly and that the nanowires effectively act as one-dimensional systems that can be characterized only by d_{nw}.[22]

Ferroelectric phase transitions were investigated by recording the time variation of the EFM signal from individual nanowires as a function of temperature (T). Figure 1c shows a series of such images obtained from a 25-nm-diameter nanowire at two different temperatures. At sufficiently low T, the signal did not decay over a period of >7 days, indicating that the nanowire was ferroelectric. At higher T, the induced polarization became metastable, decaying with time as shown in the lower panels of Figure 1c. This time-scale behavior and its interpretation as evidence of the ferroelectric phase transition is consistent with previously published electrostatic scanning probe characterizations of ferroelectric thin films at temperatures below, near, and above T_C.[23] For each wire diameter, a phase transition temperature, T_C, was identified below which the polarization was absolutely stable for the duration of the experiment (~200 h.). Although this operational definition can overestimate the true

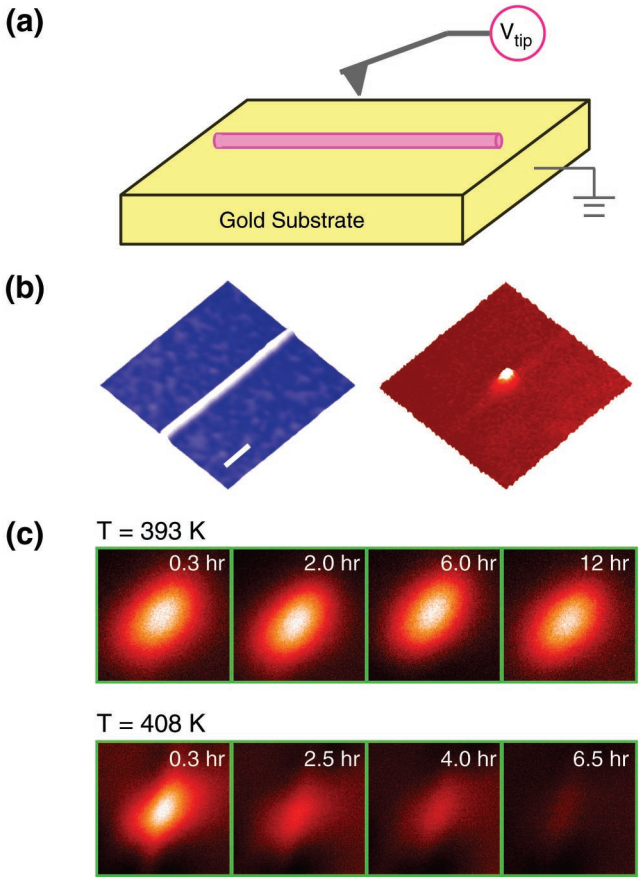

Figure 1. (a) Schematic diagram illustrating the experimental geometry. Here V_{tip} represents the voltage applied to a conductive tip. (b) A topographic image (left) and a spatial map of the electric polarization (right) of an 11-nm-diameter nanowire. The scale bar on the left image represents 200 nm. The polarization map was obtained by subtracting the electric force microscope (EFM) response at $V_{tip} = +1.5$ V from that at $V_{tip} = -1.5$ V to remove the contributions from capacitive and topological interactions between the tip and the sample. The writing of the polarization spot was performed with $V_{tip} = -10$ V. The tip−surface distance was held at 10 nm during the writing procedure and at 35 nm during the reading procedure. On the right panel, white corresponds to a resonance frequency shift ($\Delta\nu$) of 15 Hz. (c) Time series of EFM images (300 × 300 nm^2) for a 25-nm-diameter nanowire following the polarization writing below and above the phase transition temperature. The writing and reading conditions were identical to those in b.

phase transition temperature, the extrapolation of the experimentally determined T_C reproduced the bulk phase transition temperature ($T_{C,bulk}$) in the limit of large d_{nw}, substantiating the validity of the experimental procedure.

The strong dependence of T_C on d_{nw} is illustrated in Figure 2. The figure shows that T_C in larger diameter nanowires is close to $T_{C,bulk}$ (~400 K) but drops rapidly as d_{nw} decreases. Furthermore, the inset to Figure 2 clearly shows that the reduction of T_C is inversely proportional to d_{nw}. Notably, T_C reaches room temperature when d_{nw} is ~3 nm, thus establishing the smallest diameter at which a stable polarization signal can be measured at room temperature. Extrapolation of the experimental data indicates that nanowires with d_{nw} as small as 0.8 nm can support ferroelectricity at lower temperatures.

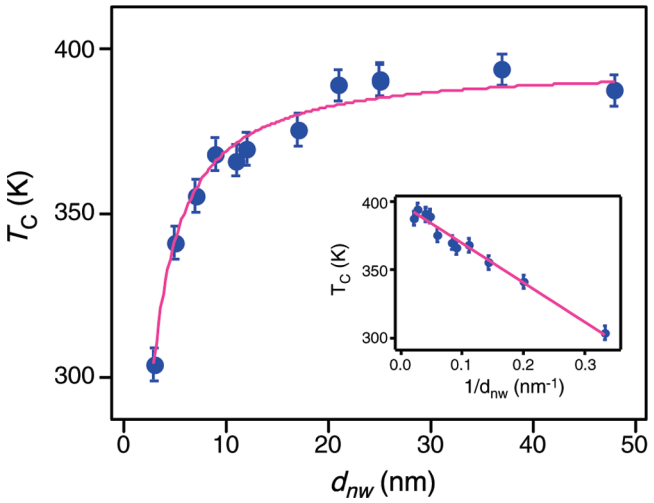

Figure 2. Ferroelectric phase transition temperature (T_C) as a function of d_{nw}. The solid circles are the experimentally determined T_C, and the error bars are uncertainties. The magenta solid line is the result of the fit to the data using the $1/d_{nw}$ scaling relation. The inset plots T_C as a function of $1/d_{nw}$ and illustrates the inverse-diameter dependence.

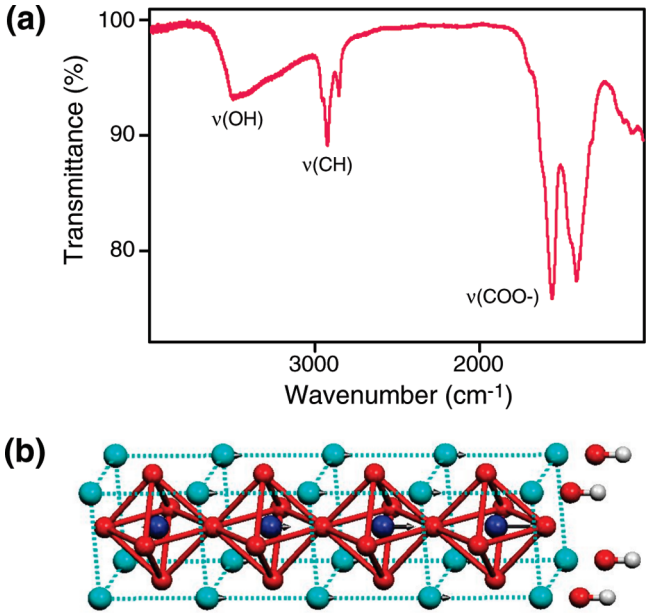

Figure 3. (a) An infrared spectrum of a $BaTiO_3$ nanowire ensemble showing bands of OH stretching (from adsorbed OH) and CH stretching modes (from oleic acid ligands). The sample was prepared in the KBr pellet form after baking the nanowire sample at 430 K in ultrahigh vacuum. The spectrum was taken under inert N_2 environment. (b) Relaxed structure for the 1.6-nm $BaTiO_3$/OH system obtained from our DFT calculations. Barium, titanium, oxygen, and hydrogen atoms are represented by cyan, blue, red, and gray, respectively. Displacements from perfect perovskite positions are shown by arrows (scaled up by a factor of 7).

The $1/d_{nw}$ scaling relation shown in Figure 2 suggests that the observed suppression of ferroelectricity is caused by the depolarizing field.[24,25] However, current views of ferroelectric destabilization with size suggest that the magnitude of this depolarizing field should become too large to support stable polarization at significantly greater values of d_{nw} than those observed in Figure 2, particularly in a geometry lacking a top metallic electrode that screens the polarization charge.[8,9,11,12] The data therefore suggest that a new screening mechanism is responsible for stabilizing nanoscale ferroelectricity in $BaTiO_3$ nanowires.

One promising candidate that may explain the observed ferroelectric stability is the adsorbate-induced charge screening. Previous studies have shown that surface hydroxylation is prevalent in oxides, including $BaTiO_3$, especially when these oxides are prepared by wet chemical methods, and that chemisorbed OH is stable in an ultrahigh-vacuum environment at elevated temperatures (>670 K).[18−20] Moreover, the $BaTiO_3$ nanowires studied here are covered with oleate ligands that are introduced during the synthesis. Figure 3a shows the infrared spectrum of the nanowire ensemble that underwent high-temperature treatment in ultrahigh vacuum and clearly illustrates the presence of OH and oleate groups on the surface of $BaTiO_3$ nanowires. These molecular adsorbates can compensate the surface polarization charges, providing a mechanism for reducing the depolarizing fields.

To assess the role of molecular and atomic adsorbates, the $BaTiO_3$ nanowires were modeled via accurate first-principles density-functional-theory (DFT) computations. DFT simulations for 0.8−4.0-nm-thick $BaTiO_3$ films were also performed using both generalized gradient (GGA) and local density approximations (LDA) to ensure that the results are not sensitive to the choice of functional.[8,9,26] Comparison of results for 0.8-nm nanowires and 0.8-nm films revealed only minor differences in adsorbate adsorption energy (0.04 eV) and ionic displacements in the oxide (<0.0025 nm), indicating that ferroelectricity in nanowires and thin films behave similarly. Both BaO- and TiO_2-terminated structures were modeled and showed very similar adsorbate-stabilized ferroelectricity. Because experimental evidence suggests that the BaO surface predominates in the nanowires,[27] we focus on this termination.

The bottom Au electrode was modeled in three different ways; as a vacuum, as a physisorbed film, and as a film forming an epitaxial interface with one $BaTiO_3$ surface. In addition to OH, atomic H and O were also considered as adsorbates, and the effect of the oleate ligands was modeled by the adsorption of HCO and HCOO (products of HCOOH molecules). All adsorbates were modeled at full coverage (one adsorbate per adsorption site) on the 1×1 $BaTiO_3$ surface, and the HCOOH-derived adsorbates were additionally simulated at half coverage on the $c(2 \times 2)$ surface. The favored adsorption site for both OH and O was determined to be directly above the surface Ba or Ti cation, while the H preferred to bind to the surface oxygen ions. The HCO fragment acted as an electropositve adsorbate, bonding to a surface oxygen ion through the carbon atom, while the electronegative HCOO preferred to form an ester linkage with a surface cation.

In all calculations, a $4 \times 4 \times 1$ Monkhorst-Pack[28] k-point mesh was used, and a vacuum of more than 2 nm separated periodic copies of the structures along the surface normal. Applying a dipole correction did not affect the structures significantly. For all systems, the entire structure was relaxed until the forces on each atom were <0.002 eV/nm. The DFT-

GGA calculations were performed using ultra-soft pseudopotentials[29] as implemented in the ab initio code Dacapo (http://fysik.dtu.dk/campos), with a plane-wave cutoff of 30 Ry. The in-plane lattice constant was fixed to the theoretical (unstrained) $BaTiO_3$ value of 0.396 nm. The optimal c parameter for the tetragonal phase of $BaTiO_3$ was determined to be 0.406 nm, the ferroelectric well depth was 28 meV/unit cell, and the polarization for the ground-state $BaTiO_3$ structure was 0.26 C/m^2. The DFT-LDA calculations were performed with our in-house plane wave code, using optimized norm-conserving pseudopotentials[30−32] with a 50 Ry cutoff. The in-plane lattice constant was fixed to 0.398 nm, and calculations with a c parameter value of 0.403 nm found a ferroelectric instability of 9 meV/unit cell, and a minimum energy polarization of 0.25 C/m^2.

The results of our simulations demonstrate unambiguously that molecules are dramatically more effective than vacuum or metal electrodes at stabilizing ferroelectricity. In agreement with previous studies,[8] none of the bare $BaTiO_3$ films considered were found to have a stable ferroelectric state; the thinnest $SrRuO_3/BaTiO_3/SrRuO_3$ film with nonzero polarization at $T = 0$ K in a recent study was 3.2 nm (8 unit cells) thick, with polarization that is a small fraction of the bulk value.[8] In contrast, our LDA and GGA calculations demonstrate that all of the $BaTiO_3$/adsorbate systems considered exhibit bulklike ferroelectricity in even the thinnest films and nanowires. Regardless of the method used to simulate the Au electrode, our results show that the electronegative adsorbates (OH, O, HCOO) stabilize a positive polarization (cations toward the surface), while the electropositive adsorbates (H, HCO) induce a negative polarization direction (cations away from the surface). Figure 3b shows a representative structure of a 1.6 nm $BaTiO_3$ film with a full coverage of OH adsorbates. As the figure illustrates, the presence of the OH adsorbates enhances ferroelectricity at the positively polarized surface, and maintains a characteristic ferroelectric displacement pattern throughout the film. Similar trends are observed in the other $BaTiO_3$/adsorbate systems, with the ferroelectric displacements enhanced at the $BaTiO_3$/adsorbate interface in all cases.

Our DFT calculations show that an overlayer of adsorbates stabilizes strong ferroelectricity throughout the nanowires, whether an Au electrode is present. This suggests that atomic or molecular adsorption screens a significant amount of the polarization charge on the surface, reducing the depolarizing field relative to bare $BaTiO_3$.

First-principles statistical mechanical analysis[16,17] demonstrates that OH, O, and H adsorbates are thermodynamically stable under experimental temperatures and pressures. We use OH adsorption as an example, as it turned out to be the most stable. For a nanowire or film in equilibrium with an atmosphere of H_2O and O_2 at fixed temperature T and pressure p, the Gibbs free energy, $\Delta G = \Delta H - T\Delta S = \Delta E + p\Delta V - T\Delta S$ can be computed for the adsorption reaction $OH(g) + BaTiO_3(s) \rightarrow BaTiO_3/OH(s)$. Here, ΔE is the chemisorption energy ($E_{chem} = E^{BaTiO_3/OH} - E^{BaTiO_3} - E^{OH}$) determined from the calculated DFT total energies for $BaTiO_3$/OH, bare $BaTiO_3$, and gas-phase OH, with correction terms for the changes in zero point and spin polarization energy upon OH adsorption. The pressure−volume term $p\Delta V$, which is dominated by the contribution of the gas-phase adsorbate, is approximated by $-k_BT$ (where k_B is the Boltzmann constant). The entropy contribution of the adsorption reaction, $T\Delta S$, is determined primarily by the difference in the vibrational entropy of the adsorbed OH and the entropy of the gas phase OH. The former is computed directly from the DFT values of the vibrational modes (found at 20, 30, 130, 470, 650, and 3860 cm^{-1}), and the latter is known experimentally and can be found tabulated online at http://webbook.nist.gov/chemistry.

The computation of ΔG as a function of temperature at the experimental H_2O and O_2 gas pressures ($p_{H_2O} = p_{O_2} \approx 10^{-12}$ atm) allows the determination of T above which OH adsorption becomes thermodynamically unstable for each film thickness. The value of this temperature ranges from 380 to 420 K depending on film thickness and is higher than the experimental value of T_C at all film thicknesses. Although our calculations show that ΔG for O and H adsorption is also favorable under some range of temperature, OH adsorption is the most favorable, indicating that sufficient OH molecules are present in the temperature and pressure range accessed in the experiment, and providing further evidence that OH-induced charge screening is responsible for the observed ferroelectric stabilization.

In summary, we determined experimentally the size scaling of nanoscale ferroelectricity in single $BaTiO_3$ nanowires. The enhanced stability relative to previous reports is explained by the presence of molecular adsorbates. The experimental strategy presented here allows the investigation of the size-dependent evolution of T_C without the complication of ensemble averaging, and it should be applicable to phase transitions of other nanoscale systems. Furthermore, the present theoretical study suggests that atomic and molecular adsorbates are more effective than metallic electrodes in stabilizing the ferroelectric stability of nanoscale domains, suggesting the possibility of new design principles for ferroelectric memory devices.

Acknowledgment. We gratefully acknowledge Qian Gu, Jun-Jieh Wang, and Xiaolin Nan for their technical assistance and scientific discussions. We also acknowledge Professors R. H. Holm and X. S. Xie for allowing access to their spectroscopy facilities. This work is supported by the National Science Foundation, the Packard Foundation, the Dreyfus Foundation (H.P.), and by the Office of Naval Research, the Center for Piezoelectric Design, and the National Science Foundation, HPCMO and DURIP (A.M.R.). J.S. acknowledges support from the Army Research Office.

References

(1) Lines, M. E.; Glass, A. M. *Principles and Applications of Ferroelectrics and Related Materials*; Clarendon Press: Oxford, 1977.
(2) Shaw, T. M.; Trolier-McKinstry, S.; McIntyre, P. C. *Annu. Rev. Mater. Res.* **2000**, *30*, 263−298.
(3) Mathews, S.; Ramesh, R.; Venkatesan, T.; Benedetto, J. *Science* **1997**, *276*, 238−240.
(4) Scott, J. F.; de Araujo, C. A. P. *Science* **1989**, *246*, 1400−1405.
(5) Ahn, C. H.; Rabe, K. M.; Triscone, J. M. *Science* **2004**, *303*, 488−491.

(6) Fong, D. D.; Stephenson, G. B.; Streiffer, S. K.; Eastman, J. A.; Auciello, O.; Fuoss, P. H.; Thompson, C. *Science* **2004**, *304*, 1650−1653.
(7) Bune, A. V.; Fridkin, V. M.; Ducharme, S.; Blinov, L. M.; Palto, S. P.; Sorokin, A. V.; Yudin, S. G.; Zlatkin, A. *Nature* **1998**, *391*, 874−877.
(8) Junquera, J.; Ghosez, P. *Nature* **2003**, *422*, 506−509.
(9) Sai, N.; Kolpak, A. M.; Rappe, A. M. *Phys. Rev. B* **2005**, *72*, 020101.
(10) Choi, K. J.; Biegalski, M.; Li, Y. L.; Sharan, A.; Schubert, J.; Uecker, R.; Reiche, P.; Chen, Y. B.; Pan, X. Q.; Gopalan, V.; Chen, L. Q.; Schlom, D. G.; Eom, C. B. *Science* **2004**, *306*, 1005−1009.
(11) Jiang, J.; Krauss, T. D.; Brus, L. E. *J. Phys. Chem. B* **2000**, *104*, 11936−11941.
(12) Tsunekawa, S.; Ito, S.; Mori, T.; Ishikawa, K.; Li, Z.-Q.; Kawazoe, Y. *Phys. Rev. B* **2000**, *62*, 3065−3070.
(13) Ahn, C. H.; Tybell, T.; Antognazza, L.; Char, K.; Hammond, R. H.; Beasley, M. R.; Fischer, Ø.; Triscone, J.-M. *Science* **1997**, *276*, 1100−1103.
(14) Kalinin, S. V.; Bonnell, D. A. *Phys. Rev. B* **2001**, *63*, 125411−23.
(15) Kalinin, S. V.; Bonnell, D. A. *Appl. Phys. Lett.* **2001**, *78*, 1116−1118.
(16) Sun, Q.; Reuter, K.; Scheffler, M. *Phys. Rev. B* **2003**, *67*, 205424.
(17) Reuter, K.; Scheffler, M. *Phys. Rev. Lett.* **2003**, *90*, 046103.
(18) Noda, T.; Wada, S.; Yano, M.; Suzuki, T. *J. Appl. Phys.* **1996**, *80*, 5223−5233.
(19) Abicht, H. P.; Voltzke, D.; Schneider, R.; Woltersdorf, J.; Lichtenberger, O. *Mater. Chem. Phys.* **1998**, *55*, 188−192.
(20) Wegmann, M.; Watson, L.; Hendry, A. *J. Am. Ceram. Soc.* **2004**, *87*, 371−377.
(21) Urban, J. J.; Yun, W. S.; Gu, Q.; Park, H. *J. Am. Chem. Soc.* **2002**, *124*, 1186−1187.
(22) Yun, W. S.; Urban, J. J.; Gu, Q.; Park, H. *Nano Lett.* **2002**, *2*, 447−450.
(23) Kalinin, S. V.; Bonnell, D. A. *J. Appl. Phys.* **2000**, *87*, 3950−3957.
(24) Dawber, M.; Chandra, P.; Littlewood, P. B.; Scott, J. F. *J. Phys.: Condens. Matter* **2003**, *15*, L393-L398.
(25) Batra, I. P.; Wurfel, P.; Silverman, B. D. *Phys. Rev. B* **1973**, *8*, 3257−3265.
(26) Kohn, W.; Sham, L. J. *Phys. Rev.* **1965**, *140*, A1133−1138.
(27) Bonnell, D. A. Private communication, 2005.
(28) Monkhorst, H. J.; Pack, J. D. *Phys. Rev. B* **1976**, *13*, 5188−92.
(29) Vanderbilt, D. *Phys. Rev. B* **1990**, *41*, 7892−7895.
(30) Rappe, A. M.; Rabe, K. M.; Kaxiras, E.; Joannopoulos, J. D. *Phys. Rev. B* **1990**, *41*, 1227−30.
(31) Ramer, N. J.; Rappe, A. M. *Phys. Rev. B* **1999**, *59*, 12471−12478.
(32) Grinberg, I.; Ramer, N. J.; Rappe, A. M. *Phys. Rev. B* **2001**, *63*, 201102.

NL052538E